 

PACS numbers: 42.55.Lt; 42.65.Ky; 42.70.Mp
DOI: 10.1070/QE2015v045n10ABEH015648

# Repetitively pulsed TEA $CO_2$ laser and its application for second harmonic generation in $ZnGeP_2$ crystal

L.V. Koval'chuk, A.N. Grezev, V.G. Niz'ev, V.P. Yakunin, V.S. Mezhevov, D.A. Goryachkin, V.V. Sergeev, A.G. Kalintsev

*Abstract.* **Experimental results are presented on the development of a radiation source emitting at a wavelength of 4.775 μm with a pulse energy up to 50 mJ and an average power up to several watts in short pulse trains. A TEA $CO_2$ laser and a nonlinear converter based on a $ZnGeP_2$ crystal, which are specially designed for these experiments, are described. The main limitations of nonlinear conversion and possible ways to overcome these limitations are considered.**

***Keywords:*** *TEA $CO_2$ laser, $ZnGeP_2$ nonlinear crystal, second harmonic generation.*

## 1. Introduction

The second harmonic of $CO_2$ laser covers the spectral range 4.6–5.4 μm, which is important for such applied problems as selective laser technologies, remote control, lidar and location systems. As a rule, as a pump source, one uses highly efficient pulsed (or repetitively pulsed) TEA $CO_2$ lasers, which can emit sub-microsecond narrow-band pulses tunable over discrete vibrational–rotational transitions of the $CO_2$ molecule within the range 9.2–10.8 μm.

The second harmonic generation (SHG) of TEA $CO_2$ laser radiation in some nonlinear crystals was experimentally demonstrated in [1–10]. The SHG efficiency reached tens of percent [1–4, 10]. The generation of the second harmonic with a relatively high pulse energy in a repetitively pulsed regime is a challenging scientific and technical problem.

The aim of the present work is to achieve the generation of the second harmonic of a TEA $CO_2$ laser at a high pulse repetition rate and a high average power.

The solution of this difficult problem includes two distinct but interrelated stages. First of all, this is the creation of a high-power repetitively pulsed TEA $CO_2$ laser with stable radiation parameters optimised from the viewpoint of highly efficient SHG. These parameters are:

**A.N. Grezev, V.G. Niz'ev, V.P. Yakunin** Institute on Laser and Information Technologies, Russian Academy of Sciences, ul. Svyatoozerskaya 1, 140700 Shatura, Moscow region, Russia; e-mail: niziev@mail.ru;
**V.S. Mezhevov** Kaluga Laser Innovation and Technology Centre, Kievskoe sh. 82, 249037 Obninsk, Kaluga region, Russia;
**D.A. Goryachkin** Russian State Scientific Center for Robotics and Technical Cybernetics, Tikhoretskii prosp. 21, 194064 St. Petersburg, Russia; e-mail: dmitrigor@mail.ru;
**V.V. Sergeev, A.G. Kalintsev** Open Joint Stock Company S.I. Vavilov State Optical Institute, Kadetskaya liniya 5, korp. 2, 199053 St. Petersburg, Russia

Received 4 August 2014; revision received 24 December 2014
Kvantovaya Elektronika **45** (10) 884–890 (2015)
Translated by M.N. Basieva

(i) high peak power and energy of pulses with a high repetition rate and a high average power;

(ii) short duration of radiation pulses with an as-short-as possible tail responsible for unwanted heating of the nonlinear crystal;

(iii) intense laser line at a wavelength determined by the nonlinear crystal;

(iv) low angular beam divergence, which must be lower than the angular phase matching width in the nonlinear crystal; and

(v) linear polarisation, whose direction is determined by the type of nonlinear interaction in the crystal used for SHG.

The second indispensable condition for the successful solution of the considered problem is the correct choice of the nonlinear crystal, its dimensions and orientation, as well as the arrangement of efficient heat removal in the case of operation with a high average power. It is also important to choose the optimal configuration of the SHG unit and the optimal scheme of pump radiation focusing into nonlinear crystals, thus optimising the parameters of the entire laser–crystal system.

In the first part of the work, we present the results on the creation and study of a repetitively pulsed high-average- and peak-power TEA $CO_2$ laser tunable over the lines of vibrational–rotational transitions of the $CO_2$ molecule. The laser is designed based on advanced components and can continuously operate for a long time. For SHG in a $ZnGeP_2$ nonlinear crystal, we used 10-min cycles of laser operation with the following parameters: 9P(20) emission line ($\lambda$ = 9.55 μm), pulse energy 0.5 J, pulse duration ~0.2 μs, and frequency up to 500 Hz.

The laser was created using the results of [11, 12] obtained with participation of the authors of the present paper. This concerns designing of the gas-dynamic circuit (GDC) and discharge chamber, as well as optimisation of the laser pulse shape for the efficient SHG by selecting the laser gas mixture composition [10].

The configuration and parameters of the second harmonic generator were chosen taking into account the experimental data of [10] on the radiation resistance and SHG efficiency of the $ZnGeP_2$ crystal, as well as the many years' experience of the manufacturer of these crystals (Laboratory of Optical Crystals Ltd., Tomsk, Russia) [13, 14].

## 2. Repetitively pulsed TEA $CO_2$ laser for SHG

The laser is designed according to the typical TEA $CO_2$ laser scheme with closed-cycle circulation of the working mixture. It consists of two main blocks, namely of laser and control blocks.

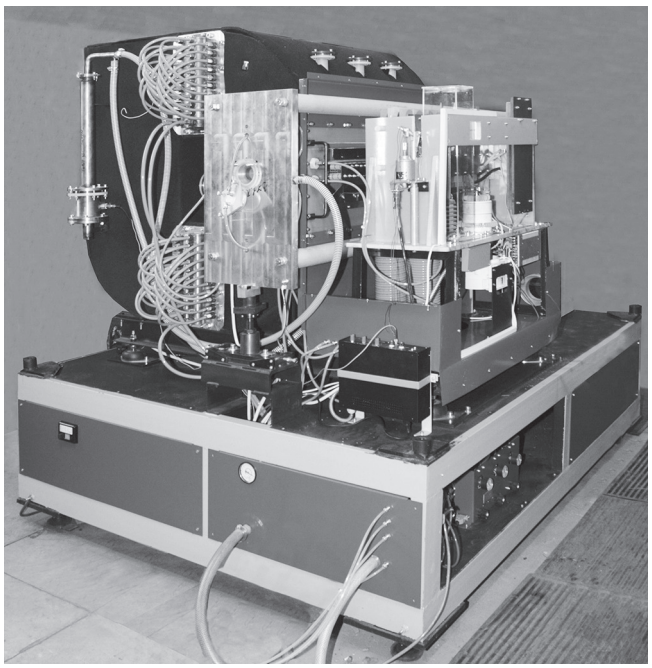

**Figure 1.** Laser module (without the outer housing).

The laser block (Fig. 1) includes:

(i) a GDC of closed-cycle laser mixture circulation with a heat exchanger and a regenerator;

(ii) a discharge chamber with the main and preionisation discharge electrodes;

(iii) a high-voltage modulator of the main discharge (MD) assembled according to the voltage doubling scheme, which includes a main-discharge capacitor bank and a thyratron;

(iv) a capacitor bank for gas preionisation prior to the application of voltage to the main-discharge electrodes;

(v) two 7020C-300-380 chargers (Optosystems Ltd., Troitsk, Russia) (Fig. 2), which charge the capacitor banks with a rate of 500 Hz and form pulses for triggering the thyratron;

(vi) a thyratron triggering and heating circuit, which ensures required parameters of high-voltage pulses for thyratron triggering; and

(v) a cavity containing a system of mirrors, a ZnSe exit window, an echelette, and systems of water and air cooling of optical element.

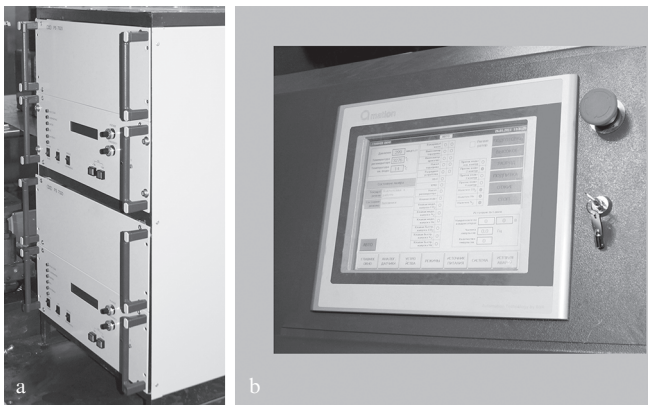


**Figure 2.** (a) Power supply and (b) touch screen control panel.

The laser block also includes:

(i) a system for the output laser beam transport, focusing, and conversion (in spatial characteristics and polarisation orientation), as well as for directing the beam on the SHG crystals; and

(ii) a second-harmonic generator consisting of $ZnGeP_2$ nonlinear crystals and the systems of temperature and phase matching angle stabilisation.

The laser is equipped with gas injection and cooling systems. They serve for cooling the thyratron, the discharge chamber electrodes, and the optical systems of the laser and second harmonic generator; for evacuating and injecting gases in the GDC prior to operation; for adding a fresh gas mixture in the process of long-term operation; and for blowing the optics inside the GDC.

All the blocks have their own housings and are additionally covered by a common removable protecting cover to ensure safe operation and low sound and electromagnetic noises. A photograph of the laser block (without the outer cover) is shown in Fig. 1. This block has overall dimensions of $2.3\times1.7\times2.5$ m and a weight of about 2 t.

The control system of the laser provides the correlation between the laser components during the setting-up procedure, in the process of operation, and after completion of the operating cycle, as well as continuous monitoring of the state of the laser systems. A photograph of the laser control panel with a touch screen is shown in Fig. 2b. The control system has dimensions of $1.2\times0.5\times1.2$ m and a weight of 90 kg.

The metal housing of the GDC (Fig. 1) contains two heat exchangers, a circulation fan with a gas consumption of $\sim1\ m^3\ s^{-1}$, and a discharge chamber, in which the gas flow rate is $\sim100\ m\ s^{-1}$. The gas circuit has windows for observation of the discharge. Care was taken to ensure vibration isolation between the mechanical systems and the optical bench of the laser.

Prior to start up, the GDC housing was evacuated to a pressure not exceeding 1 Torr and then was automatically filled with a $CO_2-N_2-He$ working mixture with a required proportion of the components up to a total pressure of, as rule, 400–500 Torr. The working mixture composition was chosen based on the recommendation of [10] on the optimisation of the SHG process. The helium concentration was 80%, while the $CO_2:N_2$ ratio was chosen within the range 4:1–6:1. A decrease in the concentration of nitrogen leads, as is known, to shortening of the laser pulse tail. The portion of radiation contained in this tail does not participate in SHG but heats the crystal.

The key unit of the TEA $CO_2$ laser is a discharge chamber with a pulsed self-sustained discharge between the cathode and anode. The discharge region size was $30\times30\times700$ mm. The UV emission of the preionisation formed by auxiliary discharges under the cathode enters the MD region through transverse slits in the central part of the cathode. To ignite a uniform self-sustained discharge in the TEA $CO_2$ laser, the capacitor bank must promptly short circuit the discharge gap. For this purpose, the capacitor bank and the high-voltage switch (thyratron) are installed in the vicinity of the discharge chamber and connected to its electrodes with the minimal induction. The discharge was supplied using a scheme of pulsed voltage doubling. The MD capacitor bank energy was 35–50 J, the shock capacitance of the MD capacitors was 0.04 μF, and the discharge current duration was 0.7–1 μs. For switching the self-sustained discharge of the laser at higher frequencies (up to 500 Hz), we used a domestic water-cooled TGI1-2500/50 thyratron. At lower frequencies (below

300 Hz), it was possible to use a more compact air-cooled TGI1-5k/50 thyratron (Pulsed Technologies Ltd, Ryazan, Russia).

The laser is based on a stable plano-concave cavity (Fig. 3). A highly reflecting concave mirror is installed inside the chamber. As a plane output coupler placed outside the chamber, we used a diffraction grating (100 lines $mm^{-1}$) with a blaze angle of 30°. The radiation is coupled out of the chamber through a Brewster window (ZnSe), i.e., is plane polarised. The diffraction grating selects one vibrational–rotational $CO_2$ laser line, as a rule, the 9P(20) line ($\lambda$ = 9.55 μm), which falls into the phase-matching region of the $ZnGeP_2$ crystal. The diffraction grating operates in the autocollimation regime in the first diffraction order. The radiation was coupled out via the zero diffraction order according to the Littrow scheme, in which the output laser beam direction is retained upon tuning the laser wavelength. The cavity mirrors and diffraction grating were mounted on water-cooled contact plates. The Brewster window and the concave mirror inside the GDC are blown over by the working gas mixture. In the case of laser operation with a high pulse repetition rate, the working mixture composition was kept constant using a regenerator and partial refreshment of the mixture from a gas vessel.

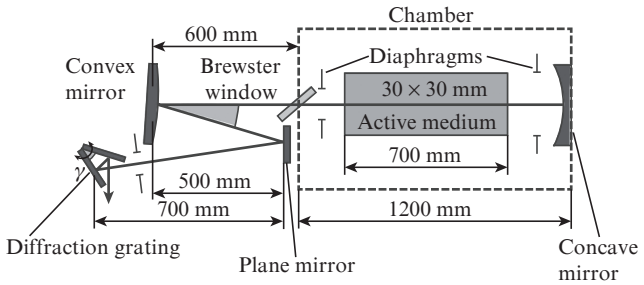


**Figure 3.** One of possible selective cavity schemes used in the laser.

## 3. Study of laser characteristics

The laser operation was tested at pulse repetition rates up to 500 Hz at a charge voltage of MD capacitors up to 25 kV and an uninterrupted operation duration up to 10 min. The laser parameters and thermal regimes stabilise for approximately this time. The radiation energy in pulsed cycles was measured by a PE-50 pyroelectric detector with the use of a calibration kit provided by the manufacturer (Ophir, Israel).

The laser cavity was usually tuned to the 9P(20) line ($\lambda$ = 9.55 μm). The experiments were mainly performed with a mixture of the composition $CO_2:N_2:He = 5:1:24$ (with a low nitrogen concentration) at a total pressure of 500 Torr. At pulse repetition rates up to 200 Hz, the pulse energy was 0.5–0.6 J and the average power was constant during the entire 10-min cycle [Fig. 4, curve (*1*)]. For comparison, note that, with the other conditions being the same, the pulse energy for the mixture $CO_2:N_2:He = 1:1:8$ exceeded 1 J.

Visually, the discharge was homogeneous during the entire pulse train, without spark discharges. To operate at higher repetition rates, it was necessary to decrease the capacitor bank voltage to 20–22 kV.

Comparing the curves in Fig. 4, one can see that the laser energy instability from pulse to pulse is higher in the case of a higher pulse repetition rate, which can be explained by the

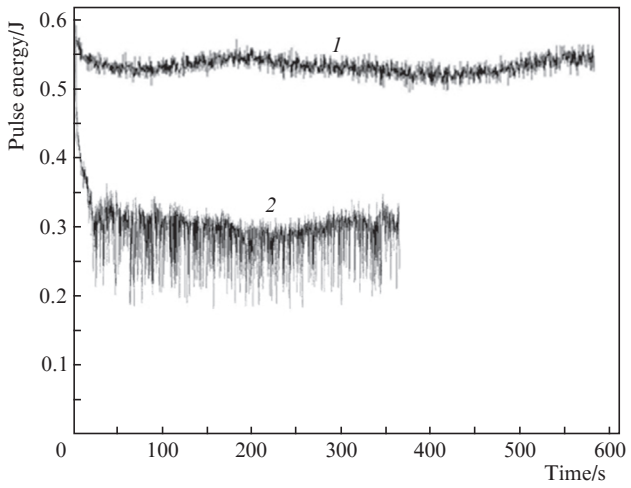


**Figure 4.** Laser pulse energy as a function of time at pulse repetition rates of (*1*) 100 and (*2*) 500 Hz.

fact that the PE-50 pyroelectric detector measured the pulse energies periodically (with a rate not exceeding 15 Hz) and the electronic circuit had no synchronisation system.

The output laser beam cross section has a rectangular shape with a size of about 16×20 mm, and the angular beam divergence is 3–3.5 diffraction limits. The laser pulse shape measured by a germanium photon drag detector (Ioffe

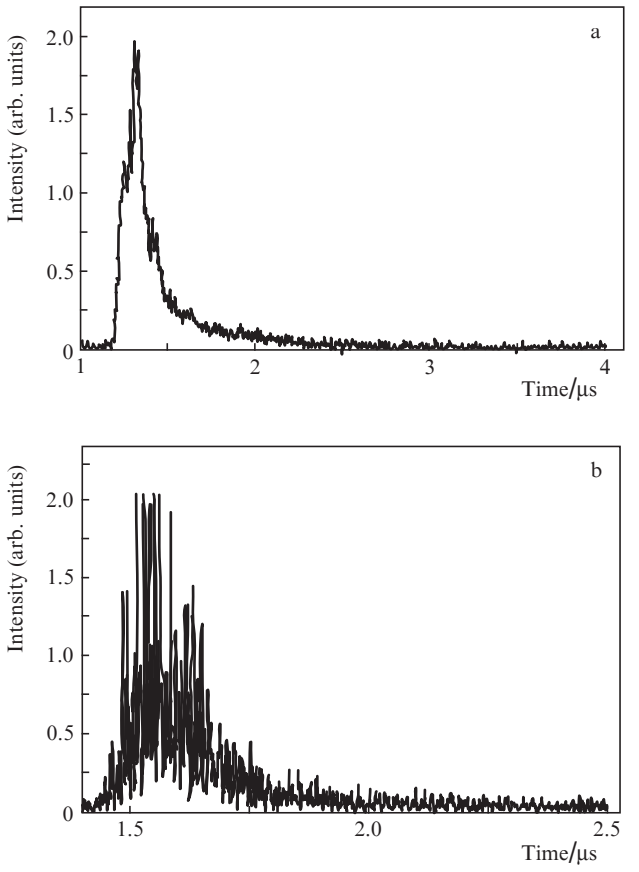


**Figure 5.** Laser pulse shape measured at oscilloscope bandwidths of (a) 20 and (b) 500 MHz. The mixture composition is $CO_2:N_2:He$ = 86:14:400 Torr.

Physico-Technical Institute, St. Petersburg, Russia) at two different oscilloscope bandwidths is shown in Fig. 5. One can see that the long pulse tail was almost completely suppressed and the peak half-width was ~200 ns. The pulse had a fine structure related to beating of longitudinal cavity modes.

## 4. Second harmonic generator

It is known that the main problems of SHG in $ZnGeP_2$ crystals in a repetitively-pulsed regime are related to a strong absorption of this crystal at a pump wavelength, which in our case was 9.55 μm. The absorption coefficients of $ZnGeP_2$ crystals presented in the literature for one and the same wavelength may differ by several times (see, for example 0.26 $cm^{-1}$ in [15] and 60 $m^{-1}$ in [2]), which is obviously determined by the growth technology, treatment and coatings of the studied crystals. The absorption coefficient for our crystals [13, 14] was measured in [10] to be ~0.4 $cm^{-1}$.

A considerable amount of heat released by the crystal volume irradiated by a laser beam can be, in principle, due to the high heat conductivity (180 mW $cm^{-1}$ $K^{-1}$ [16]), efficiently removed to the outer crystal surfaces cooled by a temperature stabilisation system.

The crystals were made in the form of parallelepipeds with dimensions 6×12×12 mm (cut angles $\theta = 66°$, $\varphi = 0$), and their broad ground faces were pressed to heat sinks (copper plates), whose temperature was controlled by Peltier elements (Fig. 6). The released heat was removed by a water-cooled heat sink. The constant-temperature regime was controlled by an electronic module using the data of temperature detectors placed near the broad faces of crystals.

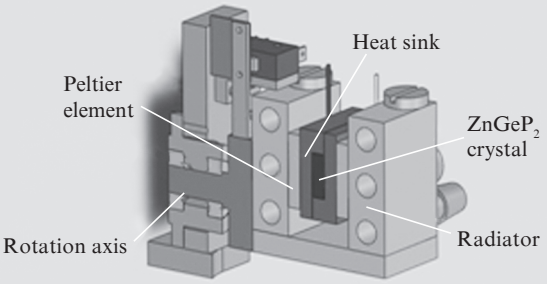


**Figure 6.** Nonlinear crystal mounting system.

The input and output faces of the crystals measuring 6×12 mm were coated by a broadband antireflection film with a reflection coefficient not exceeding 3.5%–4% in the region of both 9.55 μm and 4.775 μm. To orient the crystal at the phase-matching angle (65.2°), the temperature stabilisation unit together with the crystal was rotated with the use of step motors around the horizontal axis perpendicular to the laser beam axis (Fig. 6).

As was shown in [10], at energy densities exceeding 2 J $cm^{-2}$ (peak intensity ~20 MW $cm^{-2}$), the $ZnGeP_2$ crystals were damaged after action of 5–10 laser pulses at a repetition rate of several hertz. Because of this, in the case of operation at a high pulse repetition rate, the energy load on the crystal was decreased to 0.5–0.7 J $cm^{-2}$.

The laser beam was split into two parallel channels and coupled into the SHG unit, which contained four identical nonlinear $ZnGeP_2$ crystals (two crystals successively in each channel). In addition to a decrease in the thermal load, this geometry ensured an increase in the conversion efficiency due a larger total interaction length with simultaneous compensation for the angular divergence and the diaphragm aperture effect.

The cross sections of beams incident on the crystals of the first cascades had the form of vertically oriented ellipses with the axes of about 4 and 10 mm, which ensured lossless coupling of radiation into the crystals with cross sections of 6×12 mm. The radiation was vertically polarised (vector *E*).

After passing two frequency-conversion cascades, the second-harmonic (4.775 μm) and pump (9.55 nm) beams left the SHG unit, were superposed by mirrors into one beam, and, through a $MgF_2$ filter, which cut off the 9-μm radiation, were directed to an energy meter.

## 5. Results of SHG experiments

All the series of SHG experiments were performed with the switched-on system of cooling and temperature stabilisation of nonlinear crystals. At pulse repetition rates up to 200 Hz, the pump radiation energy at a wavelength of 9.55 μm at the entrance to the SHG unit was about 0.4 J taking into account the losses on the beam formation and splitting optical elements, i.e., the energy of the beam incident on the first crystal of each of the parallel channels was 0.2 J (average energy density ~0.5 J $cm^{-2}$). At pulse repetition rates of 300–500 Hz, the energy at the entrance to the SHG module was 30%–40% lower (Fig. 4).

The total second harmonic energy in the single-pulse regime was 40–50 mJ (with identical contributions from each channel), which corresponded to the energy conversion efficiency 10%–12%. The main contribution to the conversion was made by the first of the successive crystals in each channel (80%–85%).

Some results on SHG in a repetitively pulsed regime are presented in Fig. 7. At pulse repetition rates of 10–50 Hz, the system retained the output second harmonic pulse energy at a level of 25–30 mJ for a rather long time [more than 5 min in Fig. 7, curve (*1*)], which corresponded to an average power up to 1.5 W.

At pulse repetition rates exceeding 100 Hz, the second harmonic pulse energy decreased during the first 3–5 s and then stabilised at a level which was the lower the higher the pulse repetition rate. In particular, this level was 15–20 mJ for 100 Hz, did not exceed 5–7 mJ for 200 Hz (Fig. 7), and was 3–5 mJ for 400 Hz. In all the cases, the maximum average power was approximately the same (1.5–2 W).

Note that, after several tens of seconds of operation at repetition rates exceeding 200 Hz, we, as a rule, observed uncontrolled damage of the crystals (usually, at the entrance face of the first-cascade crystals). Because of this, at high repetition rates, we always stopped the operation after 10–15 s. The damaged crystals could be repaired by additional treatment and deposition of coatings.

## 6. Discussion of results

The experiments on SHG showed that a sufficiently high efficiency (10%–12%) was achieved only in regimes with low pulse repetition rates. With increasing pulse repetition rate and incident power, the SHG efficiency was observed to considerably decrease (Fig. 7) for several seconds. The main rea-

son for this decrease was heating of the crystals, which led to violation of the phase matching conditions. To quantitatively estimate the effect of heating on the SHG efficiency, we performed two-stage numerical calculations.

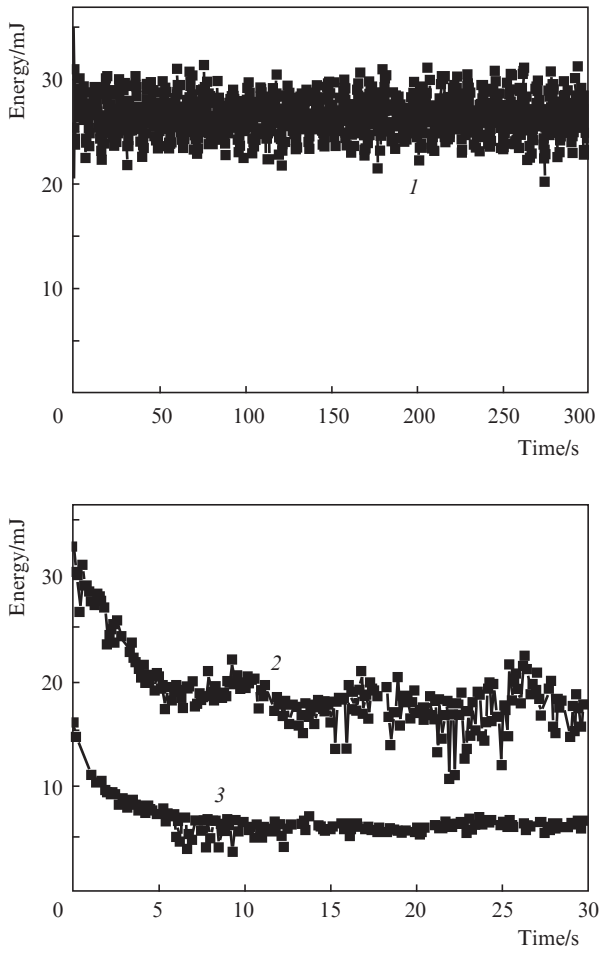


**Figure 7.** Second harmonic pulse energy dynamics at pulse repetition rates of (*1*) 10, (*2*) 100 and (*3*) 200 Hz.

First, we calculated the temperature field in the crystals by solving the stationary thermophysical problem (without allowance for SHG) for our heat sink design and experimental parameters. We determined the maximum temperature of the crystals and the temperature distribution along different directions at a fixed temperature (320 K) of the cooled faces. This temperature was chosen based on the condition of achieving steady-state and stable operation of the temperature control system.

As follows from the calculation results shown in Fig. 8, the thermal field in the crystals was strongly inhomogeneous with a maximum temperature at the laser beam axis near the entrance face and decreasing temperature in the transverse and longitudinal directions (i.e., in the direction to the cooled faces and along the laser beam propagation).

At a radiation power of 100 W at the entrance to the first crystal, the power absorbed in this crystal was ~35 W. The maximum temperature is observed near the entrance face of the crystal and is equal to 350 K, i.e., the temperature gradient between the hottest point of the crystal and the crystal faces contacting the heat sink is 30 K. The temperature in the

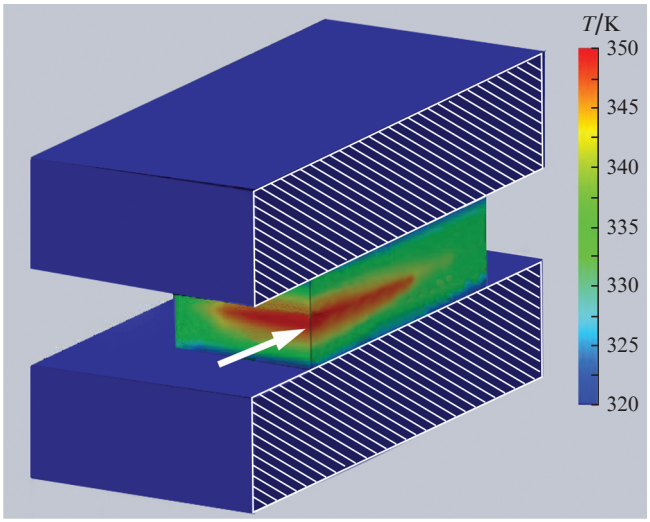


**Figure 8.** (colour online) Temperature ($T$) distribution over the cross section of the first nonlinear crystal (absorption coefficient 0.4 cm$^{-1}$). The arrow shows the direction of pump pulse propagation.

centre of the exit face of the crystal is 338 K. For the second crystal, the corresponding absorbed power and the maximum temperature gradient are 25 W and 20 K. It should be noted that, with increasing absorbed power, the temperature distribution changed only quantitatively.

Heating of the nonlinear crystals, in turn, changes the refractive index and the induced SHG phase mismatch. From the derivatives $\partial n_o/\partial T$ and $\partial n_e/\partial T$ [17, 18], we determined the temperature dependence of the phase mismatch difference $\Delta k$ ($\partial \Delta k/\partial T = 0.11 \pm 0.01$ cm$^{-1}$ K$^{-1}$). For the above-mentioned temperature gradients, the transverse difference $\Delta k$ from the entrance face centre to the side surface of the crystal is 3.3 cm$^{-1}$, while the longitudinal change $\Delta k$ along the beam axis is 1.32 cm$^{-1}$. This leads to a considerable decrease in the conversion efficiency.

Figure 9 shows the results of the second calculation stage, at which we calculated the two-cascade SHG efficiency as a function of the power absorbed by the crystals based on a modified geometrical-optical method (see details in [10, 19]) taking into account the obtained temperature distribution and the effect of additional phase mismatches. The interaction parameters were close to the corresponding parameters of the above-described experiments. For comparison, the calculations were performed for several lengths of crystals and two absorption coefficients at the laser wavelength (0.2 and 0.4 cm$^{-1}$). The absorption coefficient at the second-harmonic wavelength was taken to be 0.02 cm$^{-1}$.

From Fig. 9, one can see that, at the absorption coefficient of 0.4 cm$^{-1}$, which is typical for the crystals used in this work, the SHG efficiency was almost twice as low as it would be if we succeeded to decrease the absorption coefficient of the crystals to 0.2 cm$^{-1}$. All the crystals demonstrated a strong dependence of the SHG efficiency on heating of crystals, because of which we had to admit that it is the strong absorption of $ZnGeP_2$ nonlinear crystals that limited the possibility of obtaining efficient generation of the second harmonic of repetitively pulsed TEA $CO_2$ laser radiation in our experiments.

Note that the situation can be improved by using a two-circuit automatic system of nonlinear crystal control. In the present work, only the temperature at the side planes of the

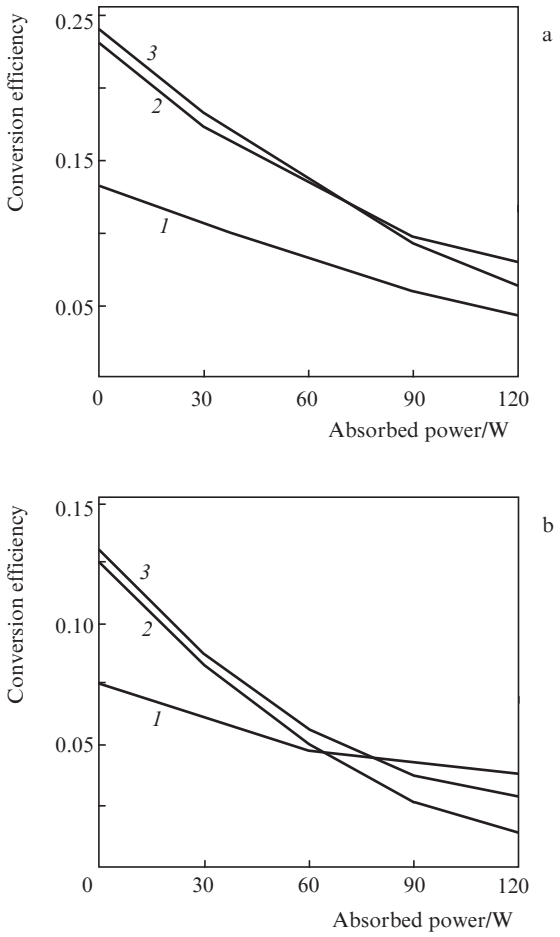


**Figure 9.** Calculated SHG efficiency for two successive crystals with lengths of (*1*) 0.5, (*2*) 1, and (*3*) 1.5 cm and absorption coefficients of (a) 0.2 and (b) 0.4 $cm^{-1}$.

crystals was maintained automatically (first circuit). The phase matching direction was corrected by a manually controlled step motor with subsequent fixation of the crystal orientation.

Nonuniform heating over the crystal cross section requires additional dynamic adjustment of phase matching (second circuit). The second circuit should control the second harmonic intensity and maintain its value in a given range by changing the crystal orientation.

The operation algorithm must be chosen taking into account that the significant (almost 20-fold) difference between the absorption coefficients at the wavelengths of the incident radiation and the second harmonic creates additional problems for thermal stabilisation of the crystal. Indeed, in the process of adjustment of the crystal heated by laser radiation to a new phase matching direction, the conversion efficiency and the second harmonic intensity increase, which, in turn, leads to a decrease in the crystal temperature due to a lower absorption of the second harmonic radiation. The phase matching conditions change again, and, as a result, the crystal temperature varies in a wave-like process, whose time constant we estimate to be several seconds.

Finally, note that interest in using $ZnGeP_2$ crystals in various nonlinear optical converters for creating lasers emitting in the range 3–5 μm does not subside in recent years. Russian researchers also have a many-year experience in such experiments and in crystal growth [3, 4, 10, 13–15, 19–21], which allows one to expect further successful works in this direction.

## 7. Conclusions

We have described a repetitively pulsed TEA $CO_2$ laser adapted for SHG in $ZnGeP_2$ crystals. Using the $CO_2:N_2:He = 5:1:24$ gas mixture operating at one lasing line with a wavelength of 9.55 μm, we obtained laser pulses with an energy of 0.3–0.5 J at repetition rates up to 500 Hz. The laser pulse duration at half maximum was ~200 ns. The laser can continually operate for a long time; the operation time for SHG was restricted to 10 min.

The possibility of SHG at a wavelength of 4.775 μm with an average power up to 1.5–2 W was demonstrated. At pulse repetition rates of 10–50 Hz, the system operated for ~5 min with a constant second harmonic pulse energy at a level of 25–30 mJ. At higher pulse repetition rates, we observed a rapid decrease in the average power and reliability of the second harmonic generator due to a possible damage of the crystals.

***Acknowledgements.*** The authors are very grateful to A.I. Gribenyukov (Laboratory of Optical Crystals Ltd., Tomsk, Russia) for providing nonlinear crystals and for fruitful discussion of the results of this work; to S.K. Vartapetov, S.N. Sergeev and V.G. Luzhnov (Optosystems Ltd., Troitsk, Russia) for providing and adjusting high-voltage sources; and to V.D. Bochkov (Pulsed Technologies Ltd., Ryazan, Russia) for providing thyratrons. We also thank N.A. Romanov, A.Yu. Rodionov, and V.P. Kalinin for their help in the work and useful discussions.

## References

1. Eckardt R.C., Fan Y.X., Byer R.L., Route R.K., Feigelson R.S., van der Laan J. *Appl. Phys. Lett.* **47**, 786 (1985).
2. Mason P.D., Jackson D.J., Gorton E.K. *Opt. Commun.*, **110**, 163 (1994).
3. Gorobets V.A., Petukhov V.O., Tochitskii S.Ya., Churakov V.V., *Optich. Zh.*, **66**, 62 (1999).
4. Andreev Yu.M., Baranov V.Yu., Voevodin V.G., Geiko P.P., Gribenyukov A.I., Izyumov C.V., Kozochkin S.M., Pis'mennyi V.D., Satov Yu.A., Strel'tsov A.P. *Kvantovaya Elektron.*, **14** (11), 2252 (1987) [*Sov. J. Quantum Electron.*, **17** (11), 1435 (1987)].
5. Isaenko L., Krinitsin P., Vedenyapin V., Yelisseyev A., Merkulov A., Zondy J.J., Petrov V. *Cryst. Growth Des.*, **5**, 1325 (2005).
6. Abdullaev G.B., Allakhverdiev K.R., Karasev M.E., Konov V.I., Kulevskii L.A., Mustafaev N.B., Pashinin P.P., Prokhorov A.M., Starodumov Yu.M., Chapliev N.I. *Kvantovaya Elektron.*, **16** (4), 757 (1989) [*Sov. J. Quantum Electron.*, **19** (4), 494 (1989)].
7. Auyeung R.C.Y., Zielke D.M., Feldman B.J. *Appl. Phys. B*, **48**, 293 (1989).
8. Menyuk N., Iseler G.W., Mooradian A. *Appl. Phys. Lett.*, **29**, 422 (1976).
9. Churnside J.H., Wilson J.J., Andreev Yu.M., Gribenyukov A.I., Shubin S.F., Dolgii S.I., Zuev V.V. In: *NOAA Technical Memorandum ERL WPL-224* (Boulder, USA, 1992) pp 1–18.
10. Koval'chuk L.V., Goryachkin D.A., Sergeev V.V., Kalintsev A.G., Kalintseva N.A., Kalinin V.P., Gribenyukov A.I. *Optich. Zh.*, **79**, 14 (2012).
11. Baranov V.Y., Dyad'kin A.P., Maluta D.D., Kuzmenko V.A., Pigulskiy S.V., Mezhevov V.S., et al. *Proc. SPIE Int. Soc. Opt. Eng.*, **4165**, 314 (2000).
12. Vasil'tsov V.V., Galushkin M.G., Golubev V.S., Niz'ev V.G., Panchenko V.Ya., Zabelin A.M., Zavalov Yu.N. *Perspekt. Mater.*, **2**, 60 (1999).

13. Verozubova G.A., Gribenyukov A.I. *Kristallogr.*, **53**, 175 (2008).
14. Gribenyukov A.I. *Opt. Atm. Okeana*, **15**, 71 (2002).
15. Andreev Yu.M., Badikov V.V., Voevodin V.G., Geiko L.G., Geiko P.P., Ivashchenko M.V., Karapuzikov A.I., Sherstov I.V. *Kvantovaya Elektron.*, **31** (12), 1075 (2001) [*Quantum Electron.*, **31** (12), 1075 (2001)].
16. Shay J.L., Wernick J.H. In: *The Science of the Solid State* (New York: Pergamon Press, 1975) Vol.7.
17. Kato K. *Appl. Opt.*, **36**, 2506 (1997).
18. Bod G.D., Buehler E., Storz F.G. *Appl. Phys. Lett.*, **18**, 301 (1971).
19. Kalintsev A.G., Kalintseva N.A., Serebryakov V.A., Kopyl'tsov A.V. *Abstracts of Papers of the XIV International Conference 'Laser Optics 2010'* (St. Petersburg, 2010).
20. Andreev Yu.M., Voevodin V.G., Gribenyukov A.I., Zyryanov O.Ya., Ippolitov I.I., Morozov A.N., Sosnin A.V., Khmel'nitskii G.S. *Kvantovaya Elektron.*, **11** (8), 1511 (1984) [*Sov. J. Quantum Electron.*, **14** (8), 1021 (1984)].
21. Andreev Yu.M., Ionin A.A., Kinyaevskii I.O., Klimachev Yu.M., Kozlov A.Yu., Kotkov A.A., Lanskii G.V., Shaiduko A.V. *Kvantovaya Elektron.*, **43** (2), 139 (2013) [*Quantum Electron.*, **43** (2), 139 (2013)].